Deep Marine Record from Sentinelle Valley (Sardinia Channel): Integrated Stratigraphy of A Key Site for Western Mediterranean Paleoceanographic and Geological Reconstruction

F. Budillon[1], F. Lirer[1], M. Iorio[1], P. Macrì[2], L. Sagnotti[1], M. Vallefuoco[1], L. Ferraro[1], S. Innangi[1], G. Di Martino[1], R. Tonielli[1]
1, Institute for Coastal Marine Environment, CNR, Napoli, Italy
2, National Institute of Geophysics and Volcanology, Roma, Italy
francesca.budillon@iamc.cnr.it

Abstract

Biotic, petrophysical, paleomagnetic proxies combined with 14C AMS data allowed us to produce, for deep marine record of Sentinelle Valley (Sardinia Channel), a detailed integrated stratigraphic time-framework for the last 80 kyr.
Major planktonic foraminiferal changes in quantitative distribution of selected climate sensitive species allowed the identification of 10 eco-biozones and the main climatic global events (Sapropel S1, Younger Dryas, Greenland Isotope Interstadial 1, Greenland Isotope Stadial 2, Heinrich events H1-H6).
An accurate age-depth profile has been proposed for the studied record which spans between 2 and 83 kyr cal. BP. The adopted age model was successively confirmed by comparing the colour reflectance data of the studied record with the astronomically tuned deep marine record ODP-Site 964 from the Ionian Sea. Three turbidite event layers were chronologically constrained within the relative low stand and lowering sea level phases associated to the MIS 4 and MIS 3.

1 Introduction

Since climate excursions recorded in Northern Hemisphere in the Greenland GISP and GRIP ice cores [1] over the last 100 kyr had more or less synchronous effects in the Mediterranean area, many researches have focused on Mediterranean marine cores, with the aim to detect their intensity and the impact on the marine environment. During the last glacial period the Mediterranean region experienced rapid modifications in hydrographic conditions in response to fast climatic excursions, known as Heinrich events (HE) and Dansgaard-Oeschger (D-O) Stadials (cold) and Interstadials (warm) [2, 3]. In particular, [4, 5] and [6] have proved that the millennial scale D-O and HE directly control the winds and precipitation system on the Northern Mediterranean basin. Even during the Holocene the principal climatic events and oscillations of the Northern Hemisphere were clearly traceable in different sectors of the Mediterranean Basin sedimentary records [5, 6, 7, 8, 9, 10, 11, 12, 13].
A detailed outline of the paleoenviron-

mental changes and their control on marine communities, calibrated by several independent proxies (tephra, sapropel, 14C geochronology), is available for the Mediterranean area (i.e. [14, 15, 16, 17, 18, 19, 9, 10], and reference therein). Several codified eco-bioevents, if clearly detected in marine records, can be used as tie points to chronologically constrain the late Pleistocene-Holocene Mediterranean marine sequences. Nevertheless, even if many reference records are available from deep-sea sites, most of them span a short time interval and lack a high resolution detail of the paleo-environmental and paleo-ecological changes before 40 kyr. Recently, [11, 12] carried out a high-resolution study of the tuned ODP-Site 977, located in the Western part of the Alboran Sea, and identified several planktonic foraminiferal eco-bioevents occurred during the marine isotope stages (MIS) 1 to 5. These eco-bioevents represent the best tool to correlate deep marine records from different Mediterranean sites.

Many recent studies emphasize the challenge when studying deep sea records to establish a reliable chronology even for the deposition of turbidites [20, 21, 15] and underline the utility to support conventional dating methodologies with different constraints. It is widely accepted that one of the main factor controlling and enhancing turbidite deposition along deep sea fan is the fall and lowstand of sea-level, whereas sea-level rise and highstand phases reduce terrigenous supply to deep sea systems [20, 22, 23].

The studied CIESM core C08 is located in the Sardinia Channel in a key position of paleoceanographic and geological significance. In fact, the Sardinia Channel connects the Alboran to the Tyrrhenian Basin and offers a stratigraphic record with the potential to link the eco-stratigraphic and paleoceanographic observations between the Western, the Central and Eastern Mediterranean late Pleistocene Holocene marine records [12, 24, 13, 25, 26]. In fact, a portion of the Modified Atlantic Water (MAW) coming from the Strait of Gibraltar [27], diverges from the part that enters the Eastern Mediterranean and flows through the Sardinia Channel into the Tyrrhenian Sea along the northern Sicilian coast [28], forming a secondary circulation gyre. The circulation system in this sector of the Tyrrhenian Sea is counter-clockwise with the Levantine Intermediate Water (LIW) inflows lapping on the northern Sicilian coast and the outflow occurring along the eastern Sardinia coast ([29] and references therein).

The core site is even in a strategic position to check the efficiency of a submarine canyon in driving density flow to the deep sea environment, even if not directly connected to any emerged sector nor to continental shelf areas [30]. Thus the possibility that such a type of canyon would form a fan can be evaluated, even verifying the significance and the timing of the turbidite deposition.

The aim of this study is to provide a record of integrated stratigraphic data spanning the last 80 kyr, relatively to a deep basin area, based on eco-biozones, 14C-dated ages, Event Stratigraphy, lithostratigraphy and petrophysical properties.

This work represents a short version of the article “Integrated stratigraphic reconstruction for the last 80 kyr in a deep sector of the Sardinia Channel (Western Mediterranean)” published on Deep - Sea Research II, v°56, 725-735 - doi:10.1016/j.dsr2.2008.07.026, by Budillon et al. (2009, [31]).

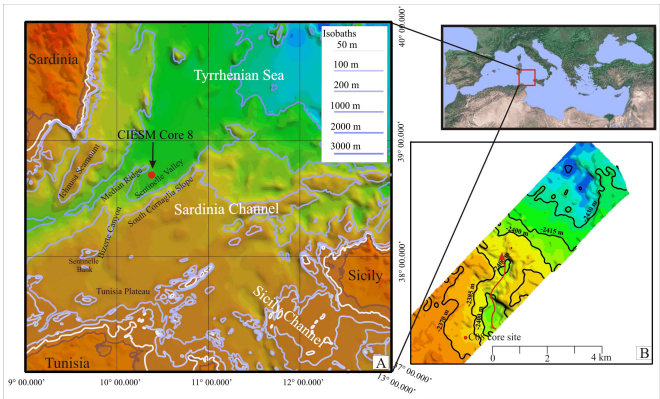

Figure 1: A) Location map of CIESM Core C08. Bathymetry from The General Bathymetric Chart of the Oceans (GEBCO, 1997); B) bathymetric detail of core site, close to a channel South-North oriented (green arrow).

2 Geological setting

The core C08 was collected in the Sentinelle Valley of the Sardinia Channel (Figure 1), during the cruise CIESM Sub2 onboard the R/V Urania in December 2005 (38°38.5364'N, 10°21.5576'E - 2370 m below sea level), and it recovered about 5.40 m of hemipelagic mud interlayered with three fine to medium sand turbidite layers of increasing thickness towards the top of the core (Figure 2). In the studied area a 400 km long submerged sector of the Apennine-Maghrebian branch of the Alpine orogen separates the Tyrrhenian (Plio-Pleistocene in age) and the Algero Provençal (Miocene in age) oceanic basins. This sector of the chain was not completely fragmented during the opening of the basins [32]. Due to the relatively minor post-orogenic extension and the good preservation of morpho-structural features, the Sardinia Channel is an important area for the reconstruction of the geodynamic evolution of the Western Mediterranean sector and was recently investigated through submersible surveys [33, 32]. The triangular shaped valley is bounded by a NE-SW oriented Median Ridge on its north-western side and by the South Cornaglia slope on the south-eastern one. The south- western sector of the Sentinelle Valley receives the sedimentary contribution of the Bizerte Canyon, which engraves the Tunisian Plateau and the south margin of the Sentinelle Bank [34]. The canyon head appears disconnected from the Tunisian shelf margin and extends over an area of about 1000 km^2 at an average depth of about 500 m (Figure 1). It represents a particular type of canyons since it is not fed by an emerged areas or by a fluvio-deltaic systems (Reading and Richards, 1994, [35, 36], but it drains a wide submarine plateau.

3 Material and methods

The physical properties of the core were measured at 1 cm step in a fully automated GEOTEK Multi-Sensor Core Logger (MSCL), in the petrophysical laborato-

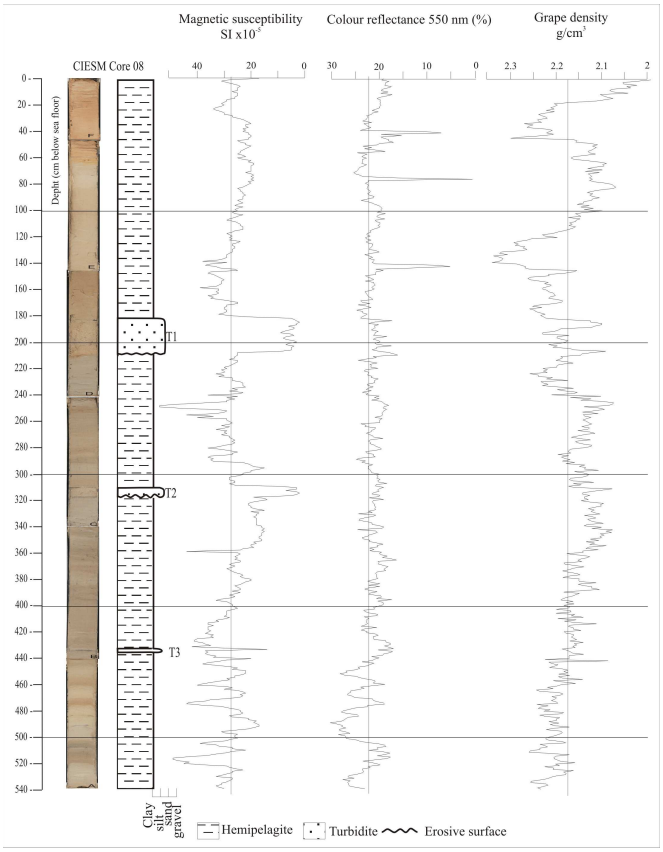

Figure 2: The core CIESM 08: photography, lithologic log, petrophysical properties curves (magnetic susceptibility, Grape density, reflectance 550 nm %) plotted against depth (cm below sea floor).

ries of IAMC in Naples (Italy). The MSCL system includes a Bartington MS2E Point sensor, to measure the low-field magnetic susceptibility (MS) with a spatial resolution of 0.4 cm and a Minolta Spectrophotometer CM 2002 which records at 0.8 cm step, the percentage of reflected energy (RSC) at 31 wavelengths in 10-nm steps, over the visible spectrum (from 400 to 700 nm).

The analysis of planktonic foraminifera was conducted on 216 samples. Sampling spacing was 2 cm from the top of the core down to the base. Each wet sample of about 20 g was dried at 50° C and washed over sieves with mesh-width size of 63 microns. Quantitative planktonic analyses were carried out on the fraction $>125\mu$m. The adopted taxonomic units were those reported by [37, 38]. According to [37] and [38], we introduced some supraspecific categories (which remain unchanged even

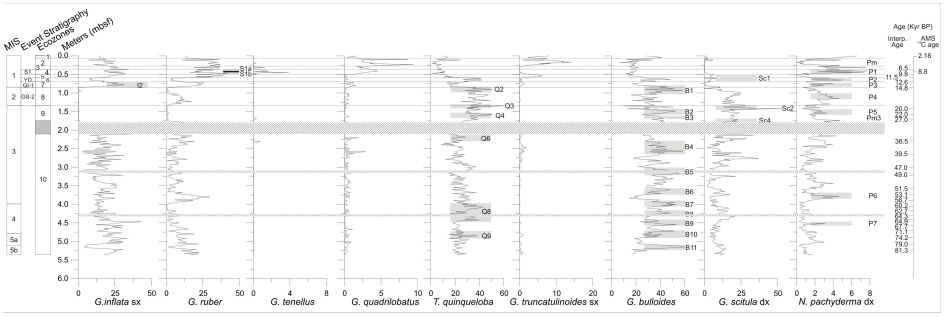

Figure 3: Relative abundance of selected planktonic foraminifera from core C08 plotted vs depth (m bsf). Eco-biozones 1 to 10 are pointed out, according to the Ecozonal scheme of [9] slightly modified. Grey bands show the selected eco-bioevents proposed by [11, 12]. Event Stratigraphy according to GRIP scheme. MIS and age scale according to [11, 12]. Associated to *G. ruber* curve, two grey bands interbedded with the black one correspond to the position of sapropel 1 equivalent with the two interval S1a and S1b. The three banded areas indicate the position of the turbidite layers.

under bad preservation conditions), reducing the number of species actually occurring in the planktonic foraminiferal assemblages.

The AMS 14C radiocarbon analysis, was performed at the CIRCE (Centre for Isotopic Research for Cultural and Environmental heritage) laboratory in Caserta (Italy). In particular, two AMS 14C analysis (at the core top and at 0.44 mbsf) were carried out on mixed planktonic foraminifera (*Globigerina bulloides* and *Globorotalia inflata*). All radiocarbon dates were corrected using a reservoir age of 48 ± 21 yr (a mean DR value calculated among six of the Tyrrhenian Sea) and calibrated using the marine data base and the CALIB 5.0 Program of [35].

4 Results: lithostratigraphy and planktonic foram

The sediment consists of hemipelagic mud, ranging in colour from reddish and ochre to light, olive and dark grey, punctuated by three turbiditic sand layers (Figure 2) from 1.82 to 2.08 m (T1), from 3.10 to 3.17 m (T2), and from 4.33 to 4.34 m (T3). The turbidite layer T1 is marked by a sharp erosive contact and consists of a thin layer of oxidized sand, and then of a massive fine to medium sand with high percentage of shell fragments; the upper boundary is sharp and the grain size populations comprised between fine sand and clay, that usually pertain to "b, c, d, e" divisions of the classical Bouma sequence [39], are missing, as evidenced by the abrupt decrease of MS and Grape density values, which are a function of grain size and lithology. A sharp contact marks the onset of the turbidite layer T2

which contains a thin layer of well sorted dark fine sand passing to a massive, well sorted bioclastic fine sand; also in this case the upper boundary is sharp and the passage from massive and structureless sand to the hemipelagic mud is abrupt. Turbidite layer T3 has well defined sharp boundaries and starts at the base with a thin layer of dark sand passing to light grey bioclastic sand. The thickness of the turbidites increases upward, but no sand layers occur in the uppermost 0.18 m of the core.

The planktonic foraminifera, characterized by modern assemblages, are abundant and well-preserved and the percentages of foraminiferal fragments are very low and do not alter the composition of the planktonic assemblage.

In terms of quantitative distribution of planktonic foraminifera a number of 13 species or groups of species were distinguished: *Globigerina bulloides* (including extremely rare specimens of *G. falconensis*), *Globigerinoides quadrilobatus* (including *G. trilobus* and very subordinate *G. sacculifer*), *G. ruber* white and pink (always extremely rare), *G. elongatus* (very rare) and *G. gomitolus* (very rare), *Globigerinoides tenellus* (rare), *Globorotalia truncatulinoides* sl. right (very rare) and left coiling, *Neogloboquadrina pachyderma* right and left coiling (extremely rare), *N. dutetrei* right and left coiling (extremely rare), *Globigerinita glutinata*, *Orbulina universa*, *Turborotalita quinqueloba*, *Globigerinatella siphoniphera* (rare) including *G. calida* (very rare), *Globoturborotalita rubescens* (rare).

The long-term trend in planktonic foraminifera reveal that the faunal composition of the studied interval does not show drastic changes in the abundance patterns (Figure 3). In particular, among the taxa that have a continuous distribution patterns, *G. bulloides*, *G. ruber*, *G. inflata* left coiled, *G. scitula* right coiled, *N. pachyderma* right coiled and *T. quinqueloba* show long-term oscillation (trend) superimposed on short-term fluctuations possibly related to high-frequency climatic oscillations (Figure 3). Among the planktonic species having discontinuous distribution, *G. quadrilobatus*, *G. truncatulinoides* left coiled and *G. tenellus* only occasionally reach significant percentages (Figure 3).

5 Planktonic foraminiferal eco-biozonation

Significant changes in quantitative distribution of the planktonic foraminifera species allowed several authors [40, 25, 38, 41, 17, 9, 15] to define eco-biozones useful for fine subdivisions of the stratigraphic record. The eco-biozone boundaries are characterized by temporary appearance or disappearance and/or evident abundance peaks of different taxa. In the present work, we refer the stratigraphic record to eco-biostratigraphic classification of [9], slightly modified. At present, the eco-biostratigraphic classification of [9]) proposes 9 eco-biozones over the last 23 kyr. In this work, we propose to mark the base of eco-biozone 9 with the strong increase of *G. inflata*, occurring in the Mediterranean area at about 30 ka [15, 13], and to extend the eco-biozone 10 back to $\sim$80 kyr. Actually, using the quantitative distribution pattern of the most abundant planktonic foraminifera species counted throughout the C08 core, we identified 10 evident eco-biozones from top to bottom (Figure 3).

The uppermost part of the studied record attributed to the eco-biozone 1, which

Events	mbsf	Age (Ka cal. BP)	References
AMS ^{14}C –	0	2,18	this work
top S1	0,360	6,5	Casford et al. (2002) (Aegean Sea)
AMS ^{14}C –	0,440	8,8	this work
base S1	0,470	9,8	Casford et al. (2002) (Aegean Sea)
topYD	0,570	11,5	Asioli et al. (2001) (Adriatic Sea)
base YD	0,700	12,6	Asioli et al. (2001) (Adriatic Sea)
base GI-1	0,850	14,8	Asioli et al. (2001) (Adriatic Sea)
base GS-2	1,350	20	Andersen et al. (2006) (Greenland Ice core)
Base B2	1.540	22	Perez-Folgado et al. (2003) (Alboran Sea)
Top B3	1.620	25.3	Perez-Folgado et al. (2004) (Alboran Sea)
Base B3	1.720	27	Perez-Folgado et al. (2003) (Alboran Sea)
Top B4	2,360	36,50	Perez-Folgado et al. (2004) (Alboran Sea)
Base B4	2,690	39.50	Perez-Folgado et al. (2004) (Alboran Sea)
Top B5	3.040	47,00	Perez-Folgado et al. (2004) (Alboran Sea)
Base B5	3,200	49,00	Perez-Folgado et al. (2004) (Alboran Sea)
Top B6	3,570	51,50	Perez-Folgado et al. (2004) (Alboran Sea)
Base B6	3,740	53,10	Perez-Folgado et al. (2004) (Alboran Sea)
Top B7	3,875	56,70	Perez-Folgado et al. (2004) (Alboran Sea)
Base B7	4.075	60,20	Perez-Folgado et al. (2004) (Alboran Sea)
Top B8	4.125	62.70	Perez-Folgado et al. (2004) (Alboran Sea)
Base B8	4.275	64.30	Perez-Folgado et al. (2004) (Alboran Sea)
Top B9	4.430	64,90	Perez-Folgado et al. (2004) (Alboran Sea)
Base B9	4.610	67,70	Perez-Folgado et al. (2004) (Alboran Sea)
Top B10	4,680	71,10	Perez-Folgado et al. (2004) (Alboran Sea)
Base B10	4,910	74,20	Perez-Folgado et al. (2004) (Alboran Sea)
Top B11	5.080	79,00	Perez-Folgado et al. (2004) (Alboran Sea)
Base B11	5.210	81,30	Perez-Folgado et al. (2004) (Alboran Sea)

Table 1: Tie-points used for age-depth profile of core C08. The *Globigerina bulloides* eco-bioevents B3 to B11 are coded according to [11, 12].

bases at 0.08 m, is characterized by a decrease in abundance of *G. quadrilobatus* and the end of *G. truncatulinoides* right coiled. This attribution is also supported by a 14C – AMS calibration, which dates 2.18 ka cal. BP (Figure 3, Table 1).

The eco-biozone 2 is defined by the concomitant abundance of *G. quadrilobatus* and *G. truncatulinoides* left and right coiled and by low abundance values of *N. pachyderma* right coiled in the lower part. Besides, the strong increase of *G. truncatulinoides* left coiled marks the base of the eco-biozone (Figure 3).

The short interval represented by eco-biozone 3, whose base is at 0.31 m, is marked by the end of micropaleontological signature of sapropel S1 and is characterized by low abundance values of *T. quinqueloba*, *G. quadrilobatus*, and *G. truncatulinoides* left coiled.

The eco-biozone 4 corresponds to the time interval of sapropel S1 deposition, although no lithological evidence was found, but for colour shades (Figure 2). *G. ruber* oscillations allowed a reliable identification of the faunal signature of the climatic events associated to the deposition of sapropel S1 (Figure 3). In particular, two distinct peaks in *G. ruber* mark the two short-term warm oscillations (S1a and S1b, [9]), separated by a cold phase between them (Figure 3). The event is supported by a 14C-AMS datum at 0.44 mbsf (within the cold phase) with an age of 8.79 ka cal. BP (Table 1) as well as an increase in abun-

dance of *G. tenellus* and *G. quadrilobatus* [9].

The eco-biozone 5 is defined by the concomitant occurrence of *G. ruber* and *G. inflata*, by a distinct peak of *G. truncatulinoides* left coiled and absence of *N. pachyderma* right coiled and very low value of *T. quinqueloba*. The eco-biozone 6 is marked by the absence of *G. ruber* and *G. inflata* left coiled, by a distinct peak of *T. quinqueloba* and of *N. pachyderma* right coiled. This eco-biozone corresponds to the Younger Dryas event, according to [9]. The eco-biozone 7 is defined by the increase in abundance of *G. ruber* and *G. inflata*, by the absence of *T. quinqueloba* and by a distinct peak of *G. quadrilobatus* and corresponds to the warmer (interstadial) GI-1. According to [9] in the eco-biozone 8 the persistent high abundance of cold species permit correlation of this interval with the GRIP GS-2 period. In particular this eco-biozone is dominated by *T. quinqueloba*, *N. pachyderma* right coiled, *G. scitula* and by absence of *G. inflata* left coiled and rare *G. ruber*. The base of this eco-biozone approximates to the base of MIS 2 [11] (Figure 3).

The eco-biozone 9 is characterized by the concomitant absence of *G. inflata* left coiled and *G. ruber*, by low abundance value of *N. pachyderma* right coiled and high abundance of *T. quinqueloba* and *G. scitula* right coiled. The eco-biozone 10 is clearly marked by the progressive downward increase in abundance of *G. inflata* left coiled and *G. ruber* and the progressive decrease of *G. scitula* right coiled, *T. quinqueloba* and *N. pachyderma* right coiled (Figure 3). No distinctive or drastic events in the planktonic faunal patterns are visible towards the base of the studied record but only short-term oscillation in *G. bulloides* (B3-B11 eco-bioevents; the adopted sampling resolution does not allow the recognition of *G. bulloides* B8 eco-bioevent), *G. inflata* left coiled (I3-I5 eco-bioevents), *T. quinqueloba* (Q4-Q9 eco-bioevents) and *N. pachyderma* right coiled (P5-P7 eco-bioevents), clearly associated to the millennial climate oscillations occurring in the last 80 kyr [12]. According to [12] close to the *G. bulloides* eco-bioevents B7 and B10 are placed the MIS 4/MIS 3 and MIS4/MIS 5a transition, respectively. Finally, according to [12] the lowermost part of the studied record lies within the eco-bioevent B11 and within the uppermost part of MIS 5b (Figure 3).

6 Age model

The identified foraminiferal marker events, regarded as to reflect major changes in oceanographic conditions and already recognised for the Central and Western Mediterranean [37, 38, 25, 24, 9, 12, 13] were used, in combination with two 14C – AMS data (Table 1), to constrain the age of core CIESM-C08 and strengthen the correlations between the Mediterranean sites. In particular, we used the age model proposed by [11, 12] for the Alboran Sea, to recognize the top and base of the eco-bioevents recorded in the core C08, the age model proposed by [25] for the Adriatic Sea, to identify the Younger Dryas and the base of the Greenland isotope interstadial 1 (GI-1) and the age model of [43] for the NGRIP record to distinguish the Greenland isotope stadial 2 (GS-2) (Table 1). The turbidite layers T1, T2 and T3 have been taken into account to construct the age model curve and to estimate the sedimentation rate. A second-order polynomial is needed to describe the age-depth relationship for the studied record, indicating an average sed-

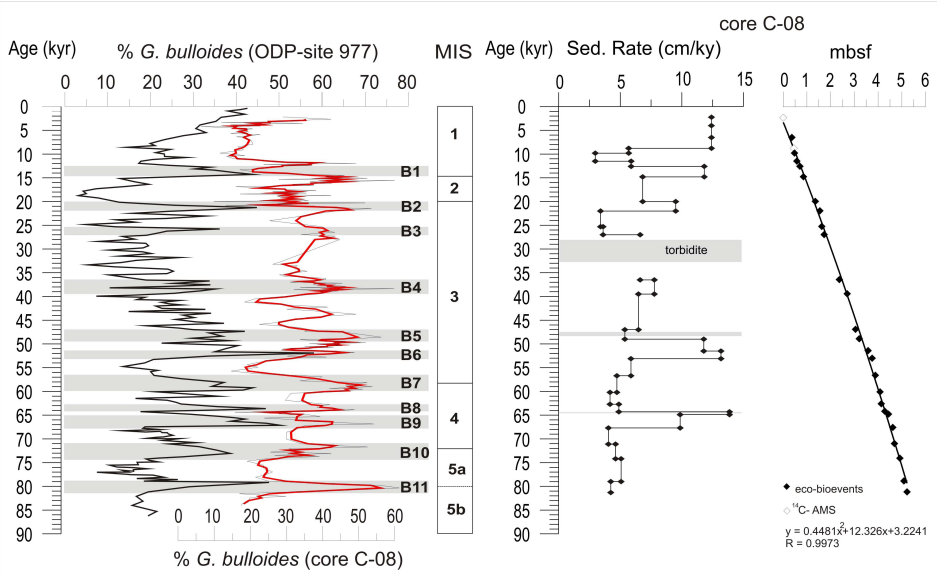

Figure 4: From left to right: comparison in time domain between the distribution pattern of *G. bulloides* from ODP-Site 977 [12] and the studied core CIESM C08 (the red curve represents a 3-points average). The grey bands and the labels B1 to B11 are from [12]. Age-Depth profile and Sedimentation Rate of core CIESM C08. The adopted tie-points by eco-bioevents and by 14C – AMS data are shown respectively with black boxes and grey boxes.

imentation rate of $\sim$7 cm·kyr^{-1} from the base to the top and four main excursions (Figure 4).

In order to confirm the reliability of the proposed age model, a three step validation process have been performed. First, the visual comparison, in time domain, between *G. bulloides* distribution pattern of [12] for the Alboran Sea and the patterns in core CIESM C08 (Figure 4), which confirmed the tuning accuracy.

The second step consisted of the comparison of the colour reflectance record at 550 nm (%) of the core CIESM C08, with the record of the ODP-Site 964 (Figure 5), drilled in the Ionian Sea at 3650 mbsl and astronomically calibrated [16]. This comparison shows that the large-scale reflectance fluctuations in core CIESM C08 not only have similar pattern to those reported in the Ionian sea record but also encompass absolute values in the same range ($\pm$10 nm). Remarkable is also the strong similarity between the colour reflectance signature of the sapropel S1 equivalent, recorded in the studied core, with the sapropel S1 colour reflectance signature in the Ionian basin. On the whole, the good visual correlation obtained between the two records supports the validity of the age model based on the identified eco-bioevents and 14C AMS calibrations.

Finally, the third control step consisted in the comparison of the *G. ruber* distri-

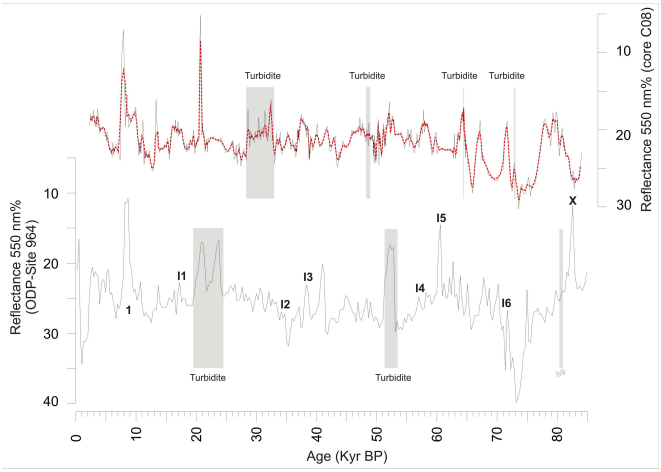

Figure 5: Comparison in time domain of colour reflectance data of core CIESM C08 (black curve, with 3 points average, red dotted curve) with reflectance data after[33] for ODP-Site 964 (thin black curve) in the Ionian Sea. The numbers I1-I6 indicate tephra layers in ODP-Site 964 and the code 1 and X indicate the position of the sapropel 1 and X, respectively.

bution pattern chronology with the δ18O NGRIP ice core record. The ecological features of *G. ruber* associated to warm and oligotrophic surface waters has been established in several oceanographic settings [44, 45, 46, 47] and it is considered an useful tool as recorders of climatic variability [48, 49, 9, 10]. The *G. ruber* and δ18O NGRIP ice core records exhibit a remarkable agreement, with the identification of the Heinrich events (H1 to H6) and of the Younger Dryas (YD) in the studied record which further support the reliability of our tuning (Figure 6).

7 Ages and provenance of turbidite events

The size population of grains, the grain fabric, the high content in bioclasts (gastropod, bivalve and echinoderm debris) and the features of the surfaces bounding T1, T2 and T3 turbidites lead us to infer a distant source of transported material, since it seems to be remobilized from high productivity areas. Both the slope of the median Ridge, and the southern Cornaglia slope can be ruled out as possible source areas for this bioclastic sand rich density currents, since their top is located respectively at about 1300 and 1000 m bsl. Namely, Sartucya 6 diving survey [33] showed that the base of the southern slope of the median Ridge (investigate from 2270 to 1940 mbsl) is draped with mud, shaped by current bedforms, while the upper slope (investigated from 1990 to 1640 m bsl) is characterized by conglomerates and sandstone layers outcropping from the mud, then volcanic rocks. The lithology pertaining to the southern Cornaglia slope has been de-

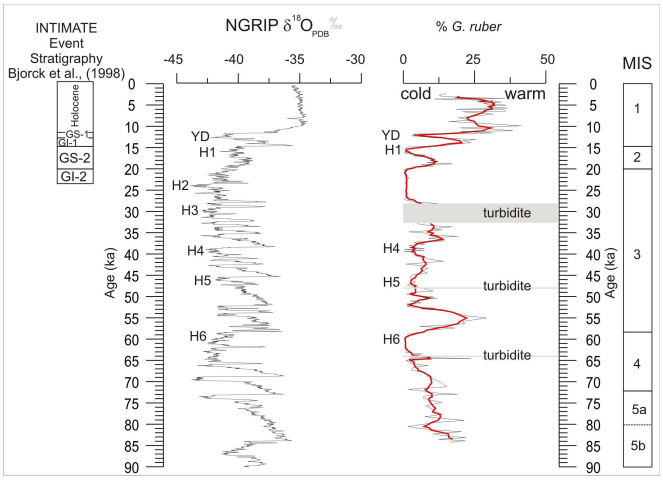

Figure 6: Distribution pattern of *G. ruber* (thin black line) with 3 points average (red line) of core CIESM C08 plotted versus δ18O NGRIP [42] record, with 7 points average, in time domain. Labels H1 to H6 indicate the position of Heinrich events and the label YD the position of the Younger Dryas.

scribed during the Sarcya 2 submersible diving [33], which evidenced the occurrence of pelagic mud along the plain (surveyed from 2500 to 2250 mbsl) and cemented coarse material in correspondence of the steep slopes (from 2250 to 2060 mbsl). Although the occurrence of several canyons along the Southern Cornaglia slope was evidenced by the bathymetric surveys [51], nevertheless they enter the Sentinelle Valley seaward to the core site and thus they possibly fed a deepest sector of the basin. Thus, we have to infer that the Bizerte Canyon may have acted as the main conduit to transport the bioclastic sand from the high productivity areas of the Tunisian plateau (Figure 1); then the flows had to cover more than 50 km before settling. As highlighted by many authors over the years [52, 53, 30] gentle gradient slopes or pre-existing slope conduits can drive very efficient density currents [54, 22] able to cover long distances in relatively "instantaneous" time and to "segregate the original grain populations into distinct and relatively well-sorted facies types with distances" [55]. The beds occurring in C08 core and in particular T1 and T2, could correspond to the facies tract F7 in [55], composed predominantly of medium to fine grained well sorted sand. In fact in this model, which associates the horizontal grain size partition of the deposit with the different degrees of flow efficiency, the F7 facies tract consists of medium to fine sand overlying a mm thick traction carpet that accounts for the development of an erosion surface at the base. This model may explain why T1 and T2 turbidites lack parallel and ripple lamination and pelitic divisions.

The turbidite layers in CIESM core C08 are confined in the lower 4 m of the core and their thickness increases upward peaking

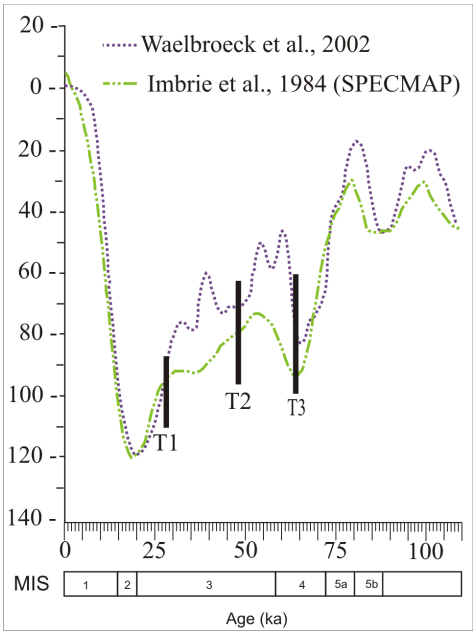

Figure 7: The inferred age of turbitite sand beds is plotted on curves of sea level variations over the last 100 kyr (from [50], modified). T2 and T3 turbidites occur during two relative lowstand phases of the MIS 4 and MIS 3, while the T1 turbidite falls during the last dropping phase of sea level of MIS 3.

at T1 (Figure 2) and pointing to a general regressive trend. Through the age model scheme of CIESM C08 core here proposed, it is possible to date T layers respectively at 28 ka cal. BP (T1), 48 ka cal. BP (T2) and 63 ka cal. BP (T3) (Figure 5), thus during the MIS 4 and MIS 3. The emplacement of T1 event bed caused the removal of an undefined thickness of hemipelagic mud correspondent to a time span of about 4 kyr (Figure 4).

Plotting their inferred age on the sea level variation curve relative to the last 100 kyr [56, 57], a strong correlation of T2 and T3 turbidite event beds deposited in this sector of the Sentinelle Valley emerges with two relative sea level low stand phases, while the T1 corresponds to the falling stage of sea level that led to the maximum sea level low stand at about 20 ka BP (Figure 7). This observation seems in agreement with the most accepted stratigraphic models of deep sea deposition [23]. Thus, the part of the basin fan intercepted by the CIESM core C08 was active and fed with bioclastic sand deposition during the relative sea level minimum and increased its transport efficiency following the sea level lowering. Nevertheless the CIESM core C08 does not record any further event of sand deposition during the maximum sea level low stand, relative to the MIS 2. A rapid starvation in detritus supply occurred in this area starting from 28 kyr and the middle fan fos-

silized below a drape of hemipelagic mud. It is reasonable to suppose that during this phase, this sector of the fan acted mainly as bypass area. In this hypothesis any possible sand flow would have been deposited basinward moving possibly through the channel showed in Figure1b.

8 Conclusions

The multidisciplinary study of core C08, recovered from the deep sector of the Sardinia Channel, based on planktonic foraminiferal assemblages and petrophysical data, provides an integrated stratigraphic reference record for the Western Mediterranean Sea that spans back for about 83 kyr. The most important eco-bioevents widely used for large scale correlation in the Western Mediterranean area were recognized providing a detailed correlation with the eco-stratigraphic reconstruction proposed by [11, 12] for the Alboran Sea.

According to [11, 12], the documented short-term oscillations in the planktonic foraminiferal fauna are clearly associated to the stadial/interstadial excursions occurring over the last 80 kyr and allowed the identification in core C08 of the S1, YD, GI-1 and GS-2 climatic events in the last 23 kyr. Furthermore, the comparison between the δ18O NGRIP ice core record with *G. ruber* oscillation of core C08, suggests the identification in the studied record of the Heinrich events (H1 to H6) and of the Younger Dryas (YD).

The eco-bioevents chronology combined with 14C – AMS data were used to define a detailed age model which was compared by means of reflectance parameters to the astronomically tuned age model proposed for the Ionian Sea ODP-Site 964 [16]. The similarity between the two reflectance records, validated the age model of the studied record especially in the time intervals between 2-25 kyr and 60-83 kyr. This methodology, if confirmed with further evidences, proved a powerful tool for reliably correlating marine records between comparable deep sea environment settings. The sector of the Sentinelle Valley intercepted by the CIESM core C08 has been sporadically fed by sand turbidite flows, likely driven along the Bizerte Canyon from the northern sector of the Tunisian Plateau, during relative sea level minimum and sea level drop of MIS 4 and 3. This sector of the basin was reached by three sand deposition events of increasing thickness in the time interval from 64 to 28 kyr cal. BP following a regressive trend. Starting from about 28 kyr this part of the fan was deactivated and fossilized beneath a carpet of hemipelagic mud at a sedimentation rate of about 7 $\mathrm{cm{\cdot}kyr^{-1}}$.

The combined logging of sedimentological and petrophysical data of core CIESM-C08, integrated with the ecobiozone stratigraphy could provide an important source of information useful to improve the confidence of correlations in the Mediterranean for the last 83 kyr.

References

[1] GRIP members. Greenland Ice-Core Project (GRIP) members, Climate instability during the last interglacial period recorded in the GRIP ice core. *Nature*, 364:203–207, 1993.

[2] H. Heinrich. Origin and consequences of cyclic ice rafting in the Northeast Atlantic Ocean during the past 130,000 years. *Quaternary Research*, 29:142–152, 1988.

[3] W. Dansgaard, S.J. Johnsen, H.B. Clausen, D. Dahl-Jensen, N.S. Gunderstrup, C.V. Hammer, C.S. Hvidberg, J.P. Steffensen, A.E. Sveinbjornsdottin, and J. Jouzel G. Bard. Evidence for general instability of past climate from a 250 kyr ice-core record. *Nature*, 364:218–220, 1993.

[4] E.J. Rohling, A. Hayes, D. Kroon, S. De Rijk, W.J. Zachariasse, and D. Eisma. Abrupt cold spells in the NW Mediterranean. *Paleoceanography*, 13:316–322, 1998.

[5] I. Cacho, J.O. Grimalt, C. Pelejero, M. Canals, F.J. Sierro, and J.A. Flores N. Shackleton. Dansgaard–Oeschger and Heinrich event imprints in Alboran Sea paleotemperatures. *Paleoceanography*, 14(6):698–705, 1999.

[6] I. Cacho, J.O. Grimalt, F.J, Sierro, and N.J. Shackleton M. Canals. Evidence for enhanced Mediterranean thermohaline circulation during rapid climate coolings. *Earth and Planetary Science Letters*, 183:417–429, 2000.

[7] I. Cacho, J.O. Grimalt, M. Canals, L. Sbaffi, N.J. Shackleton, J. Schönfeld, and R. Zahn. Variability of the western Mediterranean Sea surface temperature during the last 25,000 years and its connection with the Northern Hemisphere climatic changes. *Paleoceanography*, 16:40–52, 2001.

[8] E.J. Rohling, T.R. Cane, S. Cooke, M. Sprovieri, I. Boulabassi, K.C. Emeis, R. Schiebel, D. Kroon, F.J. Jorissen, A. Lorre, and A.E.S. Kemp. African monsoon variability during the previous interglacial maximum. *Earth and Planetary Science Letters*, 202:61–75, 2002.

[9] R. Sprovieri, E. Di Stefano, A. Incarbona, and M.E. Gargano. A high-resolution of the last deglaciation in the Sicily Channel based on foraminiferal and calcareous nannofossil quantitative distribution. *Palaeogeography, Palaeoclimatology, Palaeoecology*, 202:119–142., 2003.

[10] R. Sprovieri, E. Di Stefano, A. Incarbona, and D.W. Oppo. Suborbital climate variability during Marine Isotopic Stage 5 in the central Mediterranean basin: evidence from calcareous plankton record. *Quaternary Science Reviews*, 25:2332–2342, 2006.

[11] M. Pérez-Folgado, F.J. Sierro, J.A. Flores, I. Cacho, J.O. Grimalt, R. Zahn, and N. Shackleton. Western Mediterranean planktonic foraminifera events and millennial climatic variability during the last 70 kyr. *Marine Micropaleontology*, 1-2:49–70, 2003.

[12] M. Pérez-Folgado, F.J. Sierro, J.A. Flores, J.O. Grimalt, and R. Zahn. Paleoclimatic variations in foraminifer assemblages from the Alboran Sea (Western Mediterranean) during the last 150 ka in ODP Site 977. *Marine Geology*, 212:113–131, 2004.

[13] M. Geraga, S. Tsaila-Monopolis, C. Ioakim, G. Papatheodorou, and G. Ferentinos. Short-term climate changes in the southern Aegean Sea over the last 48,000 years. *Palaeogeography, Palaeoclimatology, Palaeoecology*, 220:311–332, 2005.

[14] G. Buccheri, G. Capretto V. Di Donato, P. Esposito G. Ferruzza T.S. Pescatore, E. Russo Ermolli, M.R. Senatore, M. Sprovieri, M. Bertoldo, D. Carella, and G. Madonna. A high resolution record of the last deglaciation in the southern Tyrrhenian Sea: environmental and climatic evolution. *Marine Geology*, 186:447–470, 2002.

[15] E. Ducassou, L. Capotondi, A. Murat, S. Bernasconi, T. Mulder, E. Gonthier, S. Migeon, J. Duprat, J. Giraudeau, and J. Mascle. Multiproxy Late Quaternary stratigraphy of the Nile deep-sea turbidite system- Towards a chronology of deep-sea terrigeneous systems. *Sedimentary Geology*, 200(1-2):1–13, 2007.

[16] L.J. Lourens. Revised tuning of Ocean Drilling Program Site 964 and KC01B (Mediterranean) and implication for the d18O, tephra, calcareous nannofossil, and geomagnetic reversal chronologies of the past 1.1 Myr. *Paleocenography*, 19:1–20, 2004.

[17] M.S. Principato, S. Giunta, C. Corselli, and A. Negri. Late Pleistocene–Holocene planktonic assemblages in three box-cores from the Mediterranean ridge area (west–southwest of Crete): palaeoecological and palaeoceanographic reconstruction of sapropel S1 interval. *Palaeogeography, Palaeoclimatology, Palaeoecology*, 190:61–77, 2003.

[18] A. Piva, A. Asioli, R.R. Schneider, F. Trincardi, N. Andersen, E. Colmenero-Hidalgo, B. Dennielou, J.A. Flores, and L. Vigliotti. Climatic cycles as expressed in sediments of the PROMESS1 borehole PRAD1-2, central Adriatic, for the last 370 ka: Integrated stratigraphy. *Geochemistry, Geophysics, Geosystems*, 9(1), 2008.

[19] E.J. Rohling, P.A. Mayewski, and P. Challenor. On the timing and mechanism of millennial-scale climate variability during the last glacial cycle. *Climate Dynamics*, 20:257–267, 2003.

[20] R.G. Walker. Turbidites and submarine fans. *Geological Association of Canada*, pages 239–263., 1992.

[21] C. Beaudouin, B. Dennielou, T. Melki, F. Guichard, N. Kallel, S. Berné, and A. Huchon. The Late-Quaternary climatic signal recorded in a deep-sea turbiditic levee (Rhône Neofan, Gulf of Lions, NW Mediterranean): palynological constraints. *Sedimentary Geology*, 172(1-2):85–97, 2004.

[22] M. Richards, M. Bowman, and H. Reading. Submarine-fan systems I: characterization and stratigraphic prediction. *Marine and Petroleum Geology*, 15(7):689–710, 1998.

[23] W.R. Normark, D.J.W. Piper, and R.N. Hiscott. Sea level control on the textural characteristics and depositional architecture of the Hueneme and associated fan systems, Santa Monica Basin, California. *Sedimentology*, 26:749–774, 1998.

[24] L. Sbaffi, F.C. Wezel, G. Curzi, and U. Zoppi. Millennial- to centennial-scale palaeoclimatic variations during Termination I and the Holocene in the central Mediterranean Sea. *Global and Planetary Change*, 40:201–217, 2004.

[25] A. Asioli, F. Trincardi, J.J. Lowe, D. Ariztegui, L. Langone, and F. Oldfield. Submillennial scale climatic oscillations in the central Adriatic during the Lateglacial. Paleoceanographic implications. *Quaternary Science Review*, 20:1201–1221, 2001.

[26] D. Ariztegui, A. Asioli, J.J. Lowe, F. Trincardi, L. Vigliotti, et al. Palaeoclimate and the formation of sapropel S1: inferences from Late Quaternary lacustrine and marine sequences in the central Mediterranean region. *Palaeogeography, Palaeoclimatology, Palaeoecology*, 158:215–240, 2000.

[27] H. L. Bryden and T. H. Kinder. Steady two-layer exchange through the Strait of Gibraltar. *Deep-Sea Research*, 38(1):445–463, 1991.

[28] C. Millot. Circulation in the western Mediterranean Sea. *Oceanology Acta*, 10:143–149, 1987.

[29] N. Pinardi and E. Masetti. Variability of the large scale general circulation of the Mediterranean Sea from observations and modelling: a review. *Palaeogeography, Palaeoclimatology, Palaeoecology*, 158:153–173., 2000.

[30] H.G. Reading and M.T. Richards. The classification of deep-water siliciclastic depositional systems by grain size and feeder system. *American Association Petroleum Geologists Bulletin*, 78:792–822, 1994.

[31] F. Budillon, F. Lirer, M. Iorio P. Macrì, L. Sagnotti, M. Vallefuoco, L. Ferraro, S. Innanzi, M. Sahabi, and R. Tonielli. Integrated stratigraphic reconstruction for the last 80 kyr in a deep sector of the Sardinia Channel (Western Mediterranean). *Deep - Sea Research II*, 2009.

[32] G.H. Mascle, P. Tricart, L. Torelli, J.P. Bouillin, R. Compagnoni, S. Depardon, J. Mascle, A. Pecher, D. Peis, F. Rekhiss, F. Rolfo, H. Bellon, G. Brocard, H. Lapierre, P. Monié, and G. Poupeau. Structure of the Sardinia Channel: crustal thinning and tardi-orogenic extension in the Apenninic-Maghrebian orogen and results of the Cyana submersible survey (SARCYA and SARTUCYA) in the Western Mediterranean. *Bull. Soc. Geol. Fr.,*, 175(6):607–627, 2004.

[33] G. Mascle, P. Tricart, J.P. Bouillin, R. Compagnoni, S. Depardon, J. Mascle, A. Pecher, D. Peis, F. Rekhiss, F. Rolfo, and L. Torelli. Données de campagne des plongées Cyana Sarcya-SartucyaEnhanced aridity and atmospheric high-pressure stability over the western Mediterranean during the North Atlantic cold events of the past 50 ky. *Geologie Alpine, Mém. H.S.,*, 34:7–113, 2001.

[34] G.H. Mascle, P. Tricart, L. Torelli, J.P. Bouillin, F. Rolfo, H. Lapierre, P. Monié, S. Depardon, J. Mascle, and D. Peis. Evolution of the Sardinia Channel (Western Mediterranean): new constraints from a diving survey on Cornacya seamount off SE Sardinia. *Marine Geology*, 179(3-4):179–201, 2001.

[35] M.A. Prins, G. Postma, J. Cleveringa, A. Cramp, and N.H. Kenyon. Controls on terrigenous supply to the Arabian Sea during the Late Quaternary: the Indus Fan. *Marine Geology*, 169:327–349, 2000.

[36] N.H. Kenyon, I. Klaucke, J. Millington, and M.K. Ivanov. Sandy submarine canyon-mouth lobes on the western margin of Corsica and Sardinia, Mediterranean Sea. *Marine Geology*, 184:69–84, 2002.

[37] F.J. Jorissen, A. Asioli, A.M. Borsetti, L. de Visser, F.J. Hilgen, E.J. Rohiling, K. van der Borg, C. Vergnaud-Grazzini, and W.J. Zachariasse. Late Quaternary central Mediterranean biochronology. *Marine Micropaleontology*, 21:169–189, 1993.

[38] L. Capotondi, A.M. Borsetti, and C. Morigi. Foraminiferal eco-biozones, a high resolution proxy for the late Quaternary biochronology in the central Mediterranean. *Marine Geology*, 153:253–274, 1999.

[39] A.H. Bouma. Sedimentology of some flysch deposits, a graphic approach to facies interpretation. page 168, 1962.

[40] A. Asioli, F. Trincardi, J.J. Lowe, and F. Oldfield. Short-term climate changes during the last Glacial-Holocene transition: comparison between Mediterranean and North Atlantic records. *Journal of Quaternary Science*, 4:3732–3781, 1999.

[41] J.S.L. Casford, E.J. Rohling, R. Abu-Zied, S. Cooke, C. Fontanier, M. Leng, and V. Lykousis. Circulation changes and nutrient concentrations in the late Quaternary Aegean Sea: A nonsteady state concept for sapropel formation. *Paleoceanography*, 17:1–11, 2002.

[42] NGRIP members. High-resolution record of Northern Hemisphere climate extending into the last interglacial period. *Nature*, 431:147–151, 2004.

[43] K.K. Andersen, A. Svensson, S.J.S.O. Johnsen Rasmussen, M. Bigler, R. Rothlisberger, U. Ruth, M.L. Siggaard-Andersen, J.P. Steffensen D. Dahl-Jensen, B.M. Vinther, and H.B.Clausen. The Greenland Ice Core Chronology 2005, 15-42 ka. Part 1: constructing the time scale. *Quaternary Science Reviews*, 25:3246–3257, 2006.

[44] C. Hemleben, M. Spindler, and O.R. Anderson. Modern Planktonic Foraminifera. page 1–363, 1989.

[45] C. Pujol and C. Vergnaud-Grazzini. Distribution patterns of live planktonic foraminifers as related to regional hydrography and productive system of the Mediterranean Sea. *Marine Micropaleontology*, 25:187–217, 1995.

[46] J.M. Watkins, A.C. Mix, and J. Wilson. Living planktic foraminifera: tracers of circulation and productivity regimes in the central equatorial Pacific. *Deep-Sea Research II*, 43:1257–1282, 1996.

[47] S. Zaric, B. Donner, G. Fischer, S. Mulitza, and G. Wefer. Sensitivity of planktic foraminifera to sea surface temperature and export production as derived from sediment trap data. *Marine Micropaleontology*, 55:75–105, 2005.

[48] R. Sprovieri. Plio-Pleistocene paleoclimatic evolution at ODP Leg 107 Site 653 (Tyrrhenian sea, Western Mediterranean). *Memorie della Società Geologica Italiana*, 44:135–144, 1991.

[49] R. Sanvoisin, S. D'Onofrio, R. Lucchi, D. Violanti, and D. Castradori. 1Ma Paleoclimatic record from the Eastern Mediterranean- Marflux Project: the first results of micropaleontological and sedimentological investigation of a long piston core from the Calabrian Ridge. *Il Quaternario*, 6:169–188, 1993.

[50] F. Antonioli, E. Bard, E.K. Potter, and S. Silenzi S. Improta. 215-ka History of sea-level oscillations from marine and continental layers in Argentarola Cave speleothems (Italy). *Global and Planetary Change*, 34(1-2):57–78, 2004.

[51] G. Brocard. Le canal de Sardaigne au Néogène: analyse morphologique et structurale. Apports de la bathymétrie multifaisceaux et des plongées Sarcya et Sartucya. *Geologie Alpine, Mém. H.S.*, 34:115–166, 2001.

[52] R.G. Walker. Turbidite sedimentary structures and their relationship to proximal and distal depositional environments. *Journal of Sedimentary Petrology*, 37(1):25–37., 1967.

[53] W. R. Normark, N. E. Barnes, and F. Coumes. Rhone Deep-Sea Fan: A review. *Geo-Marine letters,*, 3(2-4):155–160, 1984.

[54] J.E. Damuth and R.D. Flood. Morphology, sedimentation processes, and growth pattern of the Amazon Deep-Sea Fan. *Geo-Marine Letters*, 3(2-4):109–117, 1984.

[55] E. Mutti, R. Tinterri, E. Remacha, N. Mavilla, Angella, and L. Fava. An introduction to the analysis of ancient turbidite basins from an outcrop perspective. *American Association Petroleum Geologists, Continuing Education Course*, 39, 1999.

[56] C. Waelbroeck, L. Labeyrie, E. Michel, J.C. Duplessy, K. Lambeck, J.F. McManus, E. Balbon, and M. Labracherie. Sea-level and deep water temperature changes derived from benthic foraminifera isotopic records. *Quaternary Science Reviews*, 21:295– 305, 2002.

[57] J. Imbrie, J.D. Hays, D.G. Martinson, A. McIntyre, A.C. Mix, J.J. Morley, N.G. Pisias, W.L. Prell, and N.J. Shackleton. The orbital theory of Pleistocene climate: support from a revised chronology of the marine δ18O record. page 269– 305, 1984.